Dissimilar DNA Damage to Blood Lymphocytes After ^{177}Lu-Labeled DOTATOC or Prostate-Specific Membrane Antigen Therapy

Philipp Ritt[1], Camille Jobic[1], Michael Beck[1], Christian Schmidkonz[1], Torsten Kuwert[1], Michael Uder[2], and Michael Brand[2]

[1]*Clinic of Nuclear Medicine, University Hospital Erlangen, Erlangen Germany; and* [2]*Department of Radiology, University Hospital Erlangen, Erlangen, Germany*

DNA double-strand breaks in cells of radionuclide-treated patients are quantifiable by immunofluorescence microscopy, using phosphorylation of histone-variant H2AX (γ-H2AX) to mark radiation-induced foci (RIFs). Using this method, we compared excess RIFs side by side in recipients of ^{177}Lu-DOTATOC or ^{177}Lu-prostate specific membrane antigen-617 (PSMA) radioligands. We also examined relations between blood dose and dose rate, RIFs, and platelet counts. **Methods:** Venous blood samples were obtained from 48 patients subjected to ^{177}Lu-labeled radioligand therapy (^{177}Lu-DOTATOC, 26; ^{177}Lu-PSMA, 22) to quantify blood lymphocyte RIFs and blood activity concentrations at various time points, including baseline (before injection) and postinjection readings (5 min, 30 min, 4 h, 24 h, 48 h, and 72 h). Absorbed doses and dose rates to blood were derived from sequentially assessed blood activity concentrations and γ-camera imaging. Platelet levels in routine blood tests were monitored for 3 d after injection to assess responses. **Results:** RIF counts averaged 0.25 ± 0.15 at baseline. Postinjection RIF counts were significantly higher than baseline values, peaking at 5 min (average, 3.93 ± 2.51 min) and declining thereafter. Compared with RIF counts of ^{177}Lu-DOTATOC, those of ^{177}Lu-PSMA were significantly higher at 5 min after injection and significantly lower at 72 h after injection. These differences could not be fully explained by blood doses and dose rates, which were significantly higher for ^{177}Lu-PSMA than for ^{177}Lu-DOTATOC treatment at every time point. RIF counts overall correlated with dose rates across all time points (Pearson $r = 0.78$; $P < 0.01$) and with absorbed dose until 4 h after injection only (Pearson $r = 0.42$; $P < 0.01$). Declines in platelet concentration correlated significantly with RIFs at 72 h after injection (Pearson $r = -0.34$; $P < 0.05$). **Conclusion:** Although values generated by the currently used blood dosimetry model correlated with RIF counts, the difference observed in ^{177}Lu-DOTATOC and ^{177}Lu-PSMA treatment groups was unexplained. Significantly more RIFs were found in ^{177}Lu-DOTATOC recipients by comparison, despite lower dose rates and blood doses, exposing a potential limitation.

Key Words: ^{177}Lu-labeled therapy; γ-H2AX; radiation-induced foci; DOTATOC; PSMA

J Nucl Med 2021; 62:379–385
DOI: 10.2967/jnumed.120.243782

The therapeutic success of ^{177}Lu-labeled radioligands, such as ^{177}Lu-DOTATATE/DOTATOC (*1*) or ^{177}Lu-prostate-specific membrane antigen (PSMA) (*2*), has heightened interest in patient-specific dosimetry to better assess therapeutic risks and benefits. Although the merits of dosimetry are still debated (*3*), it is likely to facilitate strategic therapeutic decisions such as total injected dose or number of therapeutic cycles.

Dosimetry of ^{177}Lu-labeled compounds is largely based on imaging data that reflect doses absorbed by various organs (i.e., kidneys, liver, and spleen) or by tumors. Bone marrow dosimetry often relies on ancillary blood samples. In general, the relation between absorbed dose (by way of dosimetry) and dose-related effects has proven elusive for ^{177}Lu-labeled therapies, with few studies supporting a correlation (*3*). Several interdependent factors are perhaps involved, but insufficient standardization in imaging and dosimetry are no doubt major contributors. To optimize and unify dosimetry protocols, a cost function or metric of reasonable accuracy is needed, applicable to individual patients under routine clinical conditions and expressing the probability of tumor control or the potential for adverse effects, such as changes in blood due to bone marrow exposure.

Quantifying the phosphorylation of histone-variant H2AX (γ-H2AX) is a prospective strategy for directly assessing degrees of radiation damage to certain cell types. Using immunofluorescence microscopy, such foci mark DNA double-strand breaks (DSBs) associated with various radiologic techniques, including CT, PET/CT, and angiography (*4–12*). A significant correlation between counts of x-ray–induced γ-H2AX foci and doses delivered in vitro and in vivo has been confirmed for multiple modalities (*5,11,13–15*), with each focus representing a single DSB. The most important DNA lesions induced by ionizing radiation are DSBs. It has previously been shown in a mouse model that induction of DSBs is comparable across cell types (*12,16*). Furthermore, persistent foci have been equated with irreparable DNA damage, implicated in functional impairment of cells and even cancer induction (*17*).

Received Mar. 17, 2020; revision accepted Jun. 23, 2020.
For correspondence or reprints contact: Philipp Ritt, Clinic of Nuclear Medicine, University Hospital Erlangen, Ulmenweg 18, 91054 Erlangen, Germany.
E-mail: philipp.ritt@uk-erlangen.de
Published online Jul. 31, 2020.

Peripheral blood lymphocytes are easily obtained and are typically used to quantify γ-H2AX foci, especially in longitudinal analyses (*18*). Such radiation-induced foci (RIFs) may correlate well in hematopoietic cells and blood lymphocytes but cannot be extrapolated to other relevant cell types, such as tumor or renal cells.

Currently, there are 3 published studies (43 patients in total) applying this method to ^{177}Lu-labeled radioligand therapies (*19–21*). Two pertain to RIF counts after ^{177}Lu-DOTATATE/DOTATOC therapy (*19,21*), and one addresses RIFs after ^{177}Lu-PSMA (*20*). The present study was conducted to expand available data and knowledge through side-by-side comparison of the γ-H2AX method in ^{177}Lu-DOTATOC or ^{177}Lu-PSMA recipients. The relations between dosimetry, RIFs, and change in circulating platelet counts were also examined.

MATERIALS AND METHODS

Patient Population

Forty-eight patients receiving radioligand therapies, either ^{177}Lu-DOTATOC ($n = 26$) or ^{177}Lu-PSMA-617 (^{177}Lu-PSMA) ($n = 22$), for neuroendocrine and prostate cancer, respectively, were selected for the study. Each was treated on a compassionate-use basis between September 2015 and July 2019. The patients were hospitalized 1 d in advance of therapy to prepare for radiopharmaceutical delivery. The agents were administered intravenously over 20-min periods via an automated infusion system, retaining patients in the therapy ward for 72 h after injection (nominally) to fulfill routine dosimetry requirements. Our protocol stipulates sequential γ-camera image acquisitions and samplings of venous blood. In some patients (patients 16, 20, 40, 44, and 47), additional γ-camera acquisitions and blood samples (144 h after injection, nominally) were obtained. The institutional review board approved this study, and all subjects gave written informed consent. Further information on the patient population can be found in Table 1.

Measuring Whole-Body Time–Activity Curves

In each patient, at least 5 whole-body camera scans (Symbia T2, T6, or Intevo Bold; Siemens Healthineers) were sequentially performed within minutes after reaching full activity and then regularly at 4, 24, 48, and 72 h after injection (some at 144 h after injection as well), and a SPECT/CT scan was obtained at either 24 or 48 h after injection.

Total patient counts in the 208-keV photopeak window were derived from the geometric mean of anterior and posterior views of whole-body scans using Siemens planar analysis software (Siemens Healthineers). The decay-corrected injected activity was then divided by the first-time-point image count to yield a patient-specific calibration factor. This was used to plot a whole-body time–activity curve for each patient.

Blood Samples and Blood Time–Activity Curves

Venous blood samples (~5 mL) were drawn before ^{177}Lu-labeled radioligand administration (at baseline) and at 5 min, 30 min, 4 h, 24 h, 48 h, and 72 h after injection nominally (some at 144 h after injection) using lithium-heparin collecting tubes (S-Monovette; Sarstedt). Unfortunately, the exact time of blood sampling for the 5- and 30-min-postinjection time points was not available, because of workload and task complexity, especially at the start of infusion. Antecubital veins contralateral to sites of treatment injection were accessed. Baseline samples served for routine blood testing, reserving postinjection samples for standard dosimetry. All tubes were immediately cooled to 4°C. Later, two 1-mL samples were separated into tubes by a calibrated pipette (Pipetman G P1000G; Gilson Inc.). The remaining blood samples were stored for additional testing as necessary.

The activity concentrations (kBq/mL) of two 1-mL blood samples were determined independently via a calibrated well counter (Isomed 2100; Nuvia Instruments GmbH). Means were calculated and decay-corrected to reflect activity concentrations at the times of sample collection. These values represented patient blood time–activity curves.

Patient exposure to ionizing radiation unrelated to ^{177}Lu was minimized. Blood samples in all but 5 patients (patients 7, 9, 10, 19, and 44) were thus obtained before the SPECT/CT scan to avoid potential CT skewing of RIFs. In addition to RIF determinations, complete blood cell counts of baseline and 72-h-postinjection blood samples were performed, calculating changes in thrombocyte (platelet) counts.

Quantifying Radiation-Induced DNA Damage of Blood Lymphocytes

Small (~1.0 mL) volumes of residual sampled blood were used to determine RIF counts. The histone-variant H2AX undergoes phosphorylation (γ-H2AX) as DSBs take place, marking RIFs in blood lymphocytes. Blood samples were layered onto 6 mL of lymphocyte separation medium (1,077 g/mL; Biochrom) and centrifuged at 1,200*g* for 15 min. Separated lymphs were transferred onto glass slides by a cytocentrifuge (Cytospin; Thermo Fisher Scientific), fixed in 100% methanol (20 min, −20°C), and permeabilized in 100% acetone (1 min, −20°C). All slides were washed (3 × 10 min) in phosphate-buffered saline containing 1% fetal calf serum. The separated, washed, and methanol-fixed lymphocytes were incubated overnight at 4°C in antibody specific for γ-H2AX (1:2,500 dilution, anti-H2A.X Phospho

TABLE 1
Characteristics of Patient Population

Parameter	^{177}Lu-DOTATOC	^{177}Lu-PSMA	Combined
Patient total	26	22	48
Sex	19 M, 7 F	22 M	41 M, 7 F
Age (y)	61 ± 15	70 ± 8	65 ± 13
Injected activity (MBq)	6,420 ± 1,263*	6,300 ± 1,377*	6,365 ± 1,303*
Body mass (kg)	77 ± 17	84 ± 14	81 ± 16

*Relatively high SD is due to lower activities (~600 MBq) for 1 patient in each group to perform dosimetry only.
Qualitative data are numbers; continuous data are mean ± SD.

[Ser139] antibody; BioLegend). After being washed (3 × 10 min) in phosphate-buffered saline with 1% fetal calf serum, the slides were immersed in 2.5% formaldehyde fixative for 20 min (−20°C). Each sample was again washed (3 × 10 min) in phosphate-buffered saline with 1% fetal calf serum, followed by 1 h of incubation in Alexa Fluor 488–conjugated goat antimouse secondary antibody (1:400 dilution; Invitrogen) at room temperature. The slides were then washed (4 × 10 min) in phosphate-buffered saline (pH 7.1), and a coverslip was applied using mounting medium containing 4,6-diamidino-2-phenylindole (Vectashield; Vector Laboratories). A DM 6000 B microscope (Leica), equipped with ×63 and ×100 magnification objectives, was engaged for all fluorescence analyses. All counts were limited to 40 γ-H2AX foci. Each slide preparation was independently assessed at least 3 times by 2 masked observers, recording mean counts for subsequent analytic use. To quantify γ-H2AX foci induced by exposure, we subtracted preirradiation (background) counts from postexposure counts.

Modeling Absorbed Dose to Blood Cells

At this juncture, it was assumed that absorbed dose to whole blood and absorbed dose to blood lymphocytes were equivalent. This presumption seems justified, given the range of ^{177}Lu radiation. Furthermore, only self-irradiation of blood and total-body cross-irradiation were considered, as in previous publications (*19,20*).

Per-patient blood and total-body time–activity curves were modeled by fitting either bi- or monoexponentials to measurements, depending on the number of available sampling points (monoexponential for <4 sampling points). Time-integrated activity coefficients for blood ($\tau_{\text{mL of blood}}$ [t] in h/mL) and whole body ($\tau_{\text{total body}}$ [t] in h) were obtained by curve integration from the start of injection until time point t. For actual curve fitting and integration, standard software (Prism, version 5.04; GraphPad Software Inc.) was invoked.

Absorbed dose to blood D_{blood} (t) as a function of time was calculated using methods established elsewhere (*19*), shown in Equation 1.

$$D_{\text{blood}}(t) = A_0\left(\frac{85.3\ \text{Gy}\cdot\text{mL}}{\text{GBq}\cdot\text{h}}\cdot\tau_{\text{mL of blood}}(t) + \frac{0.00185}{m^{2/3}}\frac{\text{Gy}\cdot\text{kg}^{2/3}}{\text{GBq}\cdot h}\cdot\tau_{\text{total body}}(t)\right), \quad \text{Eq. 1}$$

where A_0 is administrated activity (GBq) and m is patient mass (kg).

Likewise, absorbed dose rate $\frac{dD}{dt}$ at each point in time was calculated as shown below. In essence, it is Equation 1, replacing time-integrated activity coefficients with activities $a_{\text{mL of blood}}$ (GBq/mL) and $a_{\text{total body}}$ (GBq), expressed as percentage of injected dose.

$$\frac{dD_{\text{blood}}}{dt}(t) = A_0\left(\frac{85.3\ \text{Gy}\cdot\text{ml}}{\text{GBq}\cdot\text{h}}\cdot a_{\text{mL of blood}}(t) + \frac{0.00185}{m^{2/3}}\frac{\text{Gy}\cdot\text{kg}^{2/3}}{\text{GBq}\cdot\text{h}}\cdot a_{\text{total body}}(t)\right). \quad \text{Eq. 2}$$

Statistical Analysis

Significant differences in baseline (background) and postinjection RIFs were assessed by Wilcoxon signed-rank testing. To compare ^{177}Lu-DOTATOC and ^{177}Lu-PSMA treatment subgroups in terms of RIFs, absorbed dose, and absorbed dose rate to blood, Mann–Whitney U testing was applied. Relations between RIFs and absorbed dose, absorbed dose rate, and reduced blood thrombocyte counts were assessed as Pearson r values. All computations relied on SPSS Statistics (version 24; IBM Corp.), setting significance at a P value of less than 0.05.

RESULTS

RIFs

The baseline (background) RIF count per cell was 0.25 ± 0.15 (mean ± SD) for all patients. Average excess RIF counts (background-subtracted) per cell were 3.93 ± 2.51 at 5 min, 3.20 ± 1.82 at 30 min, 1.67 ± 1.04 at 4 h, 0.83 ± 0.45 at 24 h, 0.53 ± 0.37 at 48 h, 0.39 ± 0.39 at 72 h, and 0.09 ± 0.04 at 144 h after ^{177}Lu-labeled radioligand injection. The RIF timeline is plotted in Figure 1. Average values by subgroup (^{177}Lu-DOTATOC and ^{177}Lu-PSMA) are listed in Supplemental Table 1 (supplemental materials are available at http://jnm.snmjournals.org).

In Wilcoxon signed-rank testing, postinjection RIF counts differed significantly from baseline values between 5 min and 48 h after injection. RIF counts at more than 48 h after injection were similar to control values, except 72 h after injection in the ^{177}Lu-DOTATOC group.

In comparing mean RIF counts after ^{177}Lu-DOTATOC or ^{177}Lu-PSMA therapy (nonparametric testing), we observed no significant groupwise difference, except at 5 min and 72 h after injection (Fig. 2). As mentioned earlier, 5 patients underwent SPECT/CT before collection of blood at 24 h after injection. In these patients, RIF counts per cell were higher at 24 h than at 4 h after injection. These data were not included in the average values reported here.

Absorbed Dose Rate to Blood

Average absorbed dose rates to the blood, calculated individually using Equation 2, were 16.36 ± 6.94 mGy/h at 1 h, 8.41 ± 4.25 mGy/h at 4 h, 1.44 ± 1.22 mGy/h at 24 h, 0.62 ± 0.50 mGy/h at 48 h, 0.33 ± 0.26 mGy/h at 72 h, and 0.10 ± 0.15 mGy/h at 144 h. Average absorbed dose rates in ^{177}Lu-DOTATOC and ^{177}Lu-PSMA treatment subgroups are provided in Supplemental Table 2. Pooled and subgroup patient data are graphed in Figures 3 and 4, respectively.

The dose rates of treatment subgroups (^{177}Lu-DOTATOC vs. ^{177}Lu-PSMA) were compared using Wilcoxon signed-rank testing. Significant differences ($P < 0.01$) were identified for all time

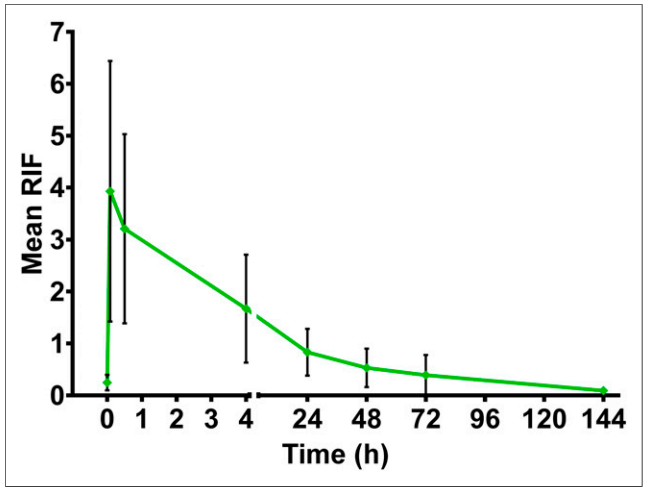

FIGURE 1. Sequential determinations of RIFs, shown as average values (background count at 0 h; all other time points already correct for background). Whiskers indicate SD. All times are nominal, after injection of ^{177}Lu-DOTATOC or ^{177}Lu-PSMA.

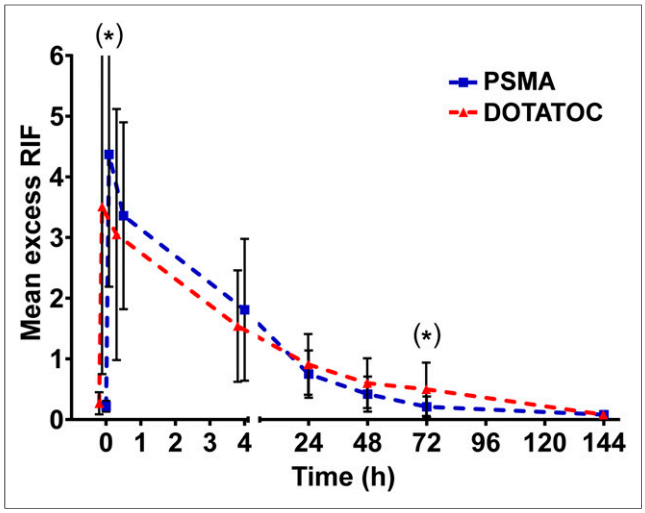

FIGURE 2. Average RIFs, shown by treatment group (background count at 0 h; all other time points already correct for background). Whiskers indicate SD. All times are nominal, after injection of ^{177}Lu-DOTATOC or ^{177}Lu-PSMA. There is slight shift in *x*-axis of ^{177}Lu-DOTATOC data at early time points to prevent visual overlap. *$P < 0.05$ (statistically significant by Mann–Whitney *U* test).

points up to 72 h. At 144 h after injection, no significant difference was observed ($P = 0.640$).

Absorbed Dose to Blood

For most patients, a biexponential fit function was applied to determine whole-body activity retention and activity retention in blood. In patient 1, a monoexponential fit function was adequate for this purpose, with respect to time. In patient 48, a monoexponential fit function was applied to activity retention in blood.

Average absorbed doses (mean ± 1 SD) to the blood, calculated individually using Equation 1, were 19.0 ± 8.3 mGy at 1 h, 54.4 ± 23.3 mGy at 4 h, 117.9 ± 62.8 mGy at 24 h, 140.1 ± 78.6 mGy at 48 h, 150.9 ± 85.1 mGy at 72 h, and 163.2 ± 89.4 mGy at 144 h. Average absorbed doses in the ^{177}Lu-DOTATOC and ^{177}Lu-PSMA treatment subgroups are provided in Supplemental Table 3. Graphs of pooled and subgroup patient data are shown as Figures 3 and 4, respectively.

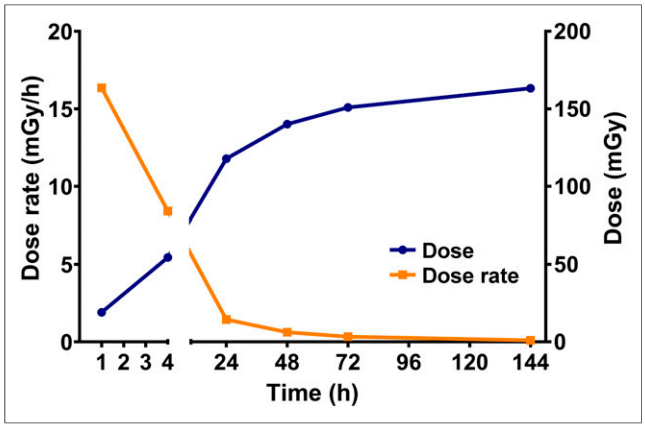

FIGURE 3. Sequential averages of absorbed dose and dose rate for patient population overall (SD omitted for clarity; Supplemental Table 2).

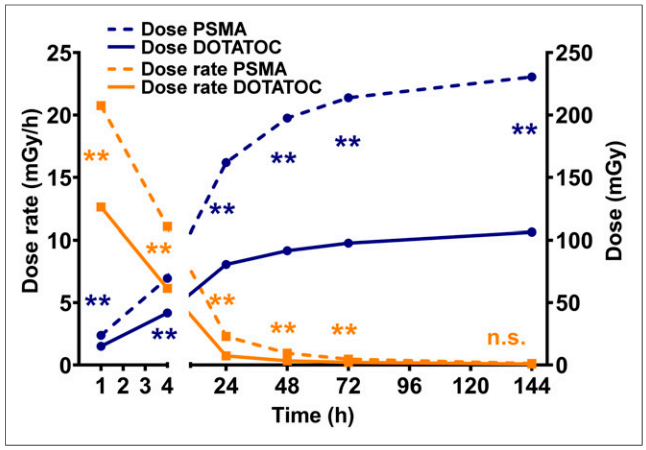

FIGURE 4. Sequential averages of absorbed doses and dose rates, shown by subgroup (SD omitted for clarity; Supplemental Table 3). **$P <$ 0.01 (highly significant groupwise difference by Wilcoxon signed-rank test). n.s. = not statistically significant.

Absorbed doses in the treatment subgroups (^{177}Lu-DOTATOC vs. ^{177}Lu-PSMA) were compared using Wilcoxon signed-rank testing. Significant differences ($P < 0.01$) were identified for all time points.

Correlation of Absorbed Dose Rate with RIFs

Figure 5A shows RIF count per cell as a function of absorbed dose rate $\frac{dD}{dt}$ in all patients, with the 2 parameters correlating significantly (Pearson $r = 0.78$; $P < 0.01$). The corresponding linear equation is as follows:

$$\text{Excess RIFs per cell} = (0.49 \pm 0.08) + (0.15 \pm 0.01)\ \text{mGy}^{-1}\text{h} \cdot \frac{dD}{dt}. \quad \text{Eq. 3}$$

Results are expressed as regression coefficient ± SE.

Dose rate and excess RIFs correlated significantly for the ^{177}Lu-DOTATOC (Pearson $r = 0.77$; $P < 0.01$) and ^{177}Lu-PSMA (Pearson $r = 0.84$; $P < 0.01$) treatment subgroups. A graph is shown in Figure 6.

The above linear correlations involved the following equations:

$$\text{DOTATOC: RIFs per cell} = (0.51 \pm 0.10) + (0.20 \pm 0.02)\ \text{mGy}^{-1} \cdot \text{h} \cdot \frac{dD}{dt} \quad \text{Eq. 4}$$

$$\text{PSMA: RIFs per cell} = (0.31 \pm 0.11) + (0.14 \pm 0.01)\ \text{mGy}^{-1} \cdot \text{h} \cdot \frac{dD}{dt} \quad \text{Eq. 5}$$

The 95% CIs for the slopes of these linear correlations were 0.17–0.23 $\text{mGy}^{-1}\cdot\text{h}$ in the ^{177}Lu-DOTATOC group and 0.12–0.16 $\text{mGy}^{-1}\cdot\text{h}$ in the ^{177}Lu-PSMA group, proving significantly different.

Correlation of Absorbed Dose with RIFs

A correlation between absorbed dose (D_{blood}) and average RIF count per cell was identified at 1 and 4 h after injection only. At later time points, no such correlation was evident. In Figure 5B, RIFs per cell is shown as a function of absorbed dose at 4 h after injection for all 48 patients (Pearson $r = 0.42$; $P < 0.01$).

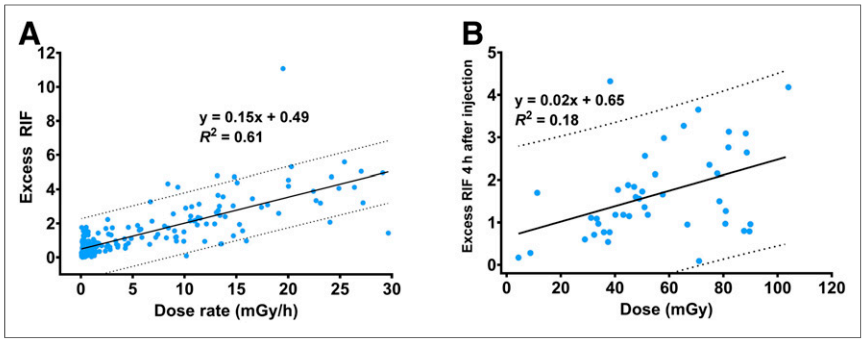

FIGURE 5. (A) Correlation between dose rate to blood and excess (background-subtracted) RIFs. All late time points (>24 h after injection) typically have low dose rates and thus appear as cluster in <2 mGy/h region. (B) Correlation between absorbed dose in blood and excess (background-subtracted) RIFs at 4 h after injection. Solid lines indicate linear model fit to data, and dashed lines indicate 95% CIs.

The corresponding linear fit yielded an R^2 of 0.18 and resulted in the following equation:

$$\text{RIFs per cell} = (0.65 \pm 0.37) + (0.018 \pm 0.006)\ \text{mGy}^{-1} \cdot D_{\text{blood}}.$$

Correlation of Change in Platelet Count with RIFs

Change in thrombocyte count (%), plotted as a function of RIF count (Fig. 7), significantly correlated with average RIF count per cell at 72 h after injection for all 48 patients (Pearson $r = -0.34$; $P < 0.05$).

The corresponding linear fit yielded an R^2 of 0.11 and resulted in the following equation:

$$\%\ \text{change in thrombocyte count} = (-4.3 \pm 2.7) - (9.9 \pm 4.9) \cdot \text{RIFs}.$$

DISCUSSION

In this study, the largest to date on this topic, we have shown the feasibility of quantifying RIFs in the blood lymphocytes of patients undergoing either ^{177}Lu-DOTATOC or ^{177}Lu-PSMA therapy. The literature on RIFs abounds because of radiographic or teletherapeutic procedures, but we know of just 3 prior studies investigating RIFs due to ^{177}Lu-labeled radionuclide therapies (*14–16*), contributing 43 patients in total. Two reports (*14,16*) have addressed ^{177}Lu-DOTATOC/DOTATE therapy in a pool of 27 patients, and another (*15*) examined 16 recipients of ^{177}Lu-PSMA. Our cohort of 48 patients is thus the largest population consecutively enrolled in a single-center study of RIFs after ^{177}Lu-labeled radioligand therapy. To facilitate comparison of results, we measured absorbed dose and dose rate as in the largest related studies heretofore conducted, by Eberlein et al. (*19*) and Schumann et al. (*20*).

Once ^{177}Lu-labeled radioligand was administered, the RIF count increased rapidly from DNA damage, peaking at 5 min (nominally) after full injection (Fig. 1). This finding is corroborated by studies involving x-ray imaging, indicating that RIF counts maximize within several minutes (*5,8,12–14*). However, other reports of ^{177}Lu-labeled pharmaceuticals seem contradictory in terms of RIFs. Denoyer et al. (*21*) have recorded maximum RIF counts for ^{177}Lu-DOTATATE at 2 h after injection and sometimes at 30 min after injection, whereas Eberlein et al. (*19*) and Schumann et al. (*20*) cite RIF maximums occurring at several hours after injection. The reason for such discrepancies is unclear.

One possible explanation is variation in the delivery procedures used. Similar to steps taken in other studies, we infused agents directly from their vials over periods of about 20 min. There was thus a gradual dilution, responsible for tapering of activity concentration after an initial peak. Because RIFs also correlate with dose rate and thus with activity concentration, a RIF peak was reached earlier by us than by other groups. In studies of other groups, large syringes of radiopharmaceuticals and syringe pumps were used, resulting in more even dispersion of activity concentration and dose rate to blood. Also, our first blood sampling (5 min after injection) was earlier than in other studies, although this 5-min time point was only nominal, since the exact time of blood sampling was not available for the 5- and 30-min-postinjection time points. Although accuracy was the aim, the actual time of blood sampling could have been delayed in many patients because of workload and task complexity at the start of infusion. In actuality, a sampling time point of between 5 and 30 min after injection was likely. Together with our slower infusion method, the 5-min time point might be comparable to a time point of about 15 min after injection in a protocol with a faster infusion rate. On the other hand, in literature comparisons of activity concentration as derived from the blood time–activity curve fit at 10 min after injection, the mean of 236 ± 108 kBq/mL in our study is similar to representative patients reported by Delker et al. (*22*) for ^{177}Lu-PSMA and Sandström et al. (*23*) for ^{177}Lu-DOTATATE. This finding could indicate that we did not considerably underestimate time-integrated activity and dose contributions from the early phase after infusion.

RIF counts gradually declined from peak levels over time (Fig. 1). However, they were significantly higher than at baseline levels at most time points tested. Only a few very late time points failed in this regard, further disadvantaged by low patient numbers. This general pattern of RIFs is affirmed in other studies (*19–21*), where RIF counts dwindle and approach pretherapeutic levels. Any disputes over whether or when baseline and late RIF counts become similar may be the fault of insufficient sampling, given the considerable interpatient variability displayed.

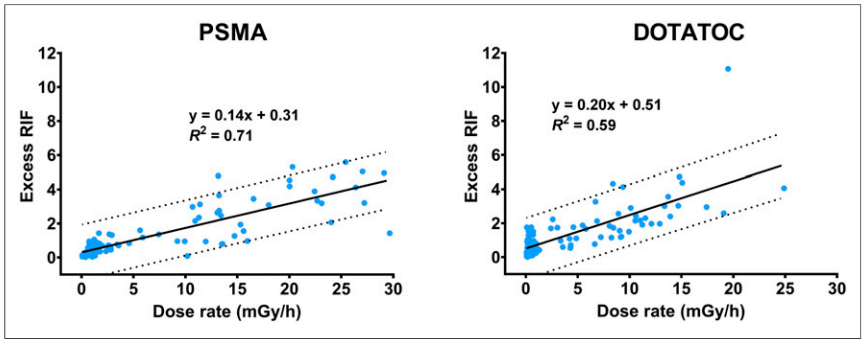

FIGURE 6. Correlations between dose rate to blood and excess (background-subtracted) RIFs in ^{177}Lu-PSMA and ^{177}Lu-DOTATOC treatment groups. All late time points (>24 h after injection) typically have low dose rates and thus appear as cluster in <2 mGy/h region. Solid lines indicate linear model fit to data, and dashed lines indicate 95% CIs.

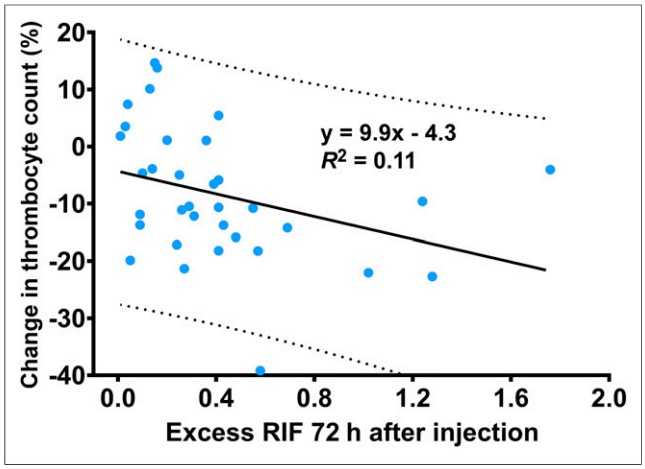

FIGURE 7. Correlation between change in blood thrombocyte count and excess (background-subtracted) RIFs at 72 h after injection. Solid lines indicate linear model fit to data, and dashed lines indicate 95% CIs.

When comparing subgroups of patients treated with ^{177}Lu-DOTATOC and ^{177}Lu-PSMA, we found the RIF count at 5 min after injection to be significantly higher for the ^{177}Lu-PSMA group, whereas at 72 h after injection, the count was significantly higher for the ^{177}Lu-DOTATOC group. Average injected activities were similar (^{177}Lu-PSMA: 6,300 ± 1,377 MBq; ^{177}Lu-DOTATOC: 6,420 ± 1,263 MBq). The higher early RIF count for ^{177}Lu-PSMA is attributable to a higher activity concentration in the blood (reflecting increased dose rate), which our data support (Fig. 4). Unfortunately, the higher RIF count for ^{177}Lu-DOTATOC at 72 h after injection is not similarly explained. In fact, the dose rate for the ^{177}Lu-DOTATOC group was lower than that for the ^{177}Lu-PSMA group at every time point. Moreover, the dose rate for ^{177}Lu-PSMA (vs. ^{177}Lu-DOTATOC) was about 60%–90% higher until 4 h after injection, whereas RIF count was only marginally higher by comparison. These inconsistencies raise the issue of a potential lapse in the dosimetry model when calculating blood dose and dose rate. For example, the current model applied here by us and regularly by others does not take into account the relatively high splenic uptake of ^{177}Lu-DOTATOC, which may add to irradiation of blood cells and raise RIF counts at later time points. Like others before us, we see that the γ-H2AX determination could help in improving and validating existing dosimetry methods and dose limits, which in turn has the potential to increase clinical acceptance of dosimetry. There is an indication that personalized, dosimetry-based dosing could lead to increased tumor doses (*24*) and better response rates (*25*). Ultimately, a 3-dimensional determination of γ-H2AX RIF by PET or SPECT, as O'Neill et al. demonstrated in a preclinical setting recently (*26*), has the potential to improve dosimetry models for many tissue types.

We found a strong and not unexpected correlation between RIF count and dose rate in all patients, as well as in ^{177}Lu-DOTATOC and ^{177}Lu-PSMA treatment subgroups. Indeed, past publications have shown that newly induced foci are repaired within reasonably short time-frames. According to Horn et al. (*18*), the decay in RIFs is biexponential, with a half-life of 1.4–1.7 h for the predominantly fast component. This time is considerably shorter than the interval between most of our sampling points. In effect, RIF totals rely heavily on numbers of continuously created foci and, thus, on dose rates. The only other study describing this effect is one by Schumann et al. (*20*), claiming such a correlation for later (≥48 h) time points only. We are unaware of any other research on the correlation of dose rate and RIF counts in the setting of ^{177}Lu-labeled radiotherapeutics.

In examining absorbed dose and RIF count, we found a correlation until 4 h after injection (no later), as is explained by ongoing reparative processes in which detectable RIFs decline as rates of repair exceed rates of injury. The absorbed dose is a monotonously rising parameter and thus will not linearly correlate with RIF counts over all time points. These tenets are supported by Eberlein et al. (*19*) and Schumann et al. (*20*), who documented linear correlations until 5 and 2.6 h after injection, respectively. A potential enhancement for the modeling of interplay between absorbed dose and RIFs might be the incorporation of repair rates, as instituted by Eberlein et al. (*19*) for ^{177}Lu-DOTATOC and Mariotti et al. (*27*) for x-ray irradiation.

It is notable that for ^{177}Lu-PSMA, absorbed dose to the blood was significantly higher in our study (0.030 ± 0.011 mGy/MBq) than in an effort by Schumann et al. (*20*) (extrapolated as ~0.0136 mGy/MBq) at comparable time points (48 h after injection). On the other hand, the absorbed dose of ^{177}Lu-DOTATOC reported here (0.017 ± 0.009 mGy/MBq) was similar to that (0.011 mGy/MBq) documented by Eberlein et al. (*19*). Because the dosimetry methods were comparable, we can only speculate about the basis for this departure in ^{177}Lu-PSMA values. Bias in determining blood activity concentration, an otherwise pivotal factor in absorbed dose to blood, is a possibility. Also, Schuman et al. used a PSMA variant (PSMA I&T; Scintomics GmbH), as opposed to our use of ^{177}Lu-PSMA-617 (ABX Advanced Biochemical Compounds), which may not share blood clearance properties. Differing patient populations may be responsible for these deviations as well. For instance, a substantially higher tumor burden in one study group would likely reduce circulating time and associated residual activity in the blood.

Ionizing radiation is a well-known cause of dose-dependent deteriorations in all hematopoietic cell lines (*28*). The time course after exposure depends on cell type. As a rule, it is quickest for lymphocytes (hours), followed by granulocytes (days), and erythrocytes (weeks). Thrombocytes and platelets decline within days after exposure (*29*). The extent to which RIF counts indicate deterministic and stochastic radiation damage is still debated (*30*). In the context of ^{177}Lu-labeled therapies, RIFs in blood lymphocytes are presumed to positively correlate with increased DNA damage, potential DNA disrepair, and functionally impaired cells. We have also shown that the dose rate in blood, which is chiefly driven by blood activity concentration, correlates with RIFs. One may therefore assume that RIF increments in blood lymphocytes are indicative of damage to other hematopoietic cells and their derivatives. In our patient population, we did find a significant negative correlation ($P < 0.05$) between short-term decline (3 d of follow-up) in thrombocyte counts of peripheral blood and RIF counts of lymphocytes, suggesting that damage on a microscopic level (number of DSBs) may eventually impact a macroscopic system (blood parameters). Only one other study has seemingly corroborated this observation. Denoyer et al. describe a relation between peak RIF counts in the first 4 h after injection and changing numbers of peripheral blood lymphocytes (*21*). Unfortunately, we could not test for therapy-related blood lymphocyte changes, because complete blood cell counts with differentials were unavailable in most of our patients.

CONCLUSION

The current dosimetry model for blood cells generates values that correlate strongly with RIFs and thus DSBs, viewed as the chief

mechanism of cell damage due to ionizing radiation. However, the ^{177}Lu-DOTATOC (vs. ^{177}Lu-PSMA) treatment group showed significantly higher and apparently contradictory RIF counts that defy standard dosimetry. Another correlation observed between RIFs and declining platelet counts indicates that microscopic damage (DSB-dependent) will eventually undermine a macroscopic system (blood parameters).

DISCLOSURE

Philipp Ritt has received honoraria for lectures from Siemens. Michael Beck has received honoraria for lectures from Bayer. Torsten Kuwert has received honoraria for lectures and grants from Siemens. Michael Uder has received honoraria for lectures and grants from Siemens, Bayer, Bracco and Medtronic. The Clinic of Nuclear Medicine in Erlangen (Philipp Ritt, Camille Jobic, Michael Beck, Christian Schmidkonz, and Torsten Kuwert) has a research cooperation with Siemens on the field of SPECT/CT but not related to the data contained in this article. No other potential conflict of interest relevant to this article was reported.

KEY POINTS

QUESTION: Is the standard blood dosimetry model sufficient for explaining the number of observed DSBs?

PERTINENT FINDINGS: Although dose rates as calculated using the standard model and DSBs correlate well, significant differences between PSMA and DOTATOC with regard to the DSB–dose relationship were found. When compared with the PSMA group, DSB number determined in DOTATOC patients was higher than predicted by standard blood dosimetry.

IMPLICATIONS FOR PATIENT CARE: These findings indicate that the currently used standard blood dosimetry model has shortcomings in calculating dose values fully representative of the actually deposited dose and, thus, of DNA damage occurring under radiotherapy with ^{177}Lu-DOTATOC and ^{177}Lu-PSMA.

REFERENCES

1. Strosberg J, El-Haddad G, Wolin E, et al. Phase 3 trial of ^{177}Lu-dotatate for midgut neuroendocrine tumors. *N Engl J Med.* 2017;376:125–135.
2. Rahbar K, Ahmadzadehfar H, Kratochwil C, et al. German multicenter study investigating ^{177}Lu-PSMA-617 radioligand therapy in advanced prostate cancer patients. *J Nucl Med.* 2017;58:85–90.
3. Cremonesi M, Ferrari ME, Bodei L, et al. Correlation of dose with toxicity and tumour response to ^{90}Y- and ^{177}Lu-PRRT provides the basis for optimization through individualized treatment planning. *Eur J Nucl Med Mol Imaging.* 2018;45:2426–2441.
4. Grudzenski S, Kuefner MA, Heckmann MB, Uder M, Lobrich M. Contrast medium-enhanced radiation damage caused by CT examinations. *Radiology.* 2009;253:706–714.
5. Kuefner MA, Grudzenski S, Hamann J, et al. Effect of CT scan protocols on x-ray-induced DNA double-strand breaks in blood lymphocytes of patients undergoing coronary CT angiography. *Eur Radiol.* 2010;20:2917–2924.
6. Kuefner MA, Grudzenski S, Schwab SA, et al. DNA double-strand breaks and their repair in blood lymphocytes of patients undergoing angiographic procedures. *Invest Radiol.* 2009;44:440–446.
7. Kuefner MA, Hinkmann FM, Alibek S, et al. Reduction of x-ray induced DNA double-strand breaks in blood lymphocytes during coronary CT angiography using high-pitch spiral data acquisition with prospective ECG-triggering. *Invest Radiol.* 2010;45:182–187.
8. Löbrich M, Rief N, Kuhne M, et al. In vivo formation and repair of DNA double-strand breaks after computed tomography examinations. *Proc Natl Acad Sci USA.* 2005;102:8984–8989.
9. Nazarov IB, Smirnova AN, Krutilina RI, et al. Dephosphorylation of histone gamma-H2AX during repair of DNA double-strand breaks in mammalian cells and its inhibition by calyculin A. *Radiat Res.* 2003;160:309–317.
10. Rogakou EP, Pilch DR, Orr AH, Ivanova VS, Bonner WM. DNA double-stranded breaks induce histone H2AX phosphorylation on serine 139. *J Biol Chem.* 1998; 273:5858–5868.
11. Rothkamm K, Balroop S, Shekhdar J, Fernie P, Goh V. Leukocyte DNA damage after multi-detector row CT: a quantitative biomarker of low-level radiation exposure. *Radiology.* 2007;242:244–251.
12. Rothkamm K, Lobrich M. Evidence for a lack of DNA double-strand break repair in human cells exposed to very low x-ray doses. *Proc Natl Acad Sci USA.* 2003;100: 5057–5062.
13. Brand M, Sommer M, Achenbach S, et al. X-ray induced DNA double-strand breaks in coronary CT angiography: comparison of sequential, low-pitch helical and high-pitch helical data acquisition. *Eur J Radiol.* 2012;81:e357–e362.
14. Kuefner MA, Brand M, Ehrlich J, Braga L, Uder M, Semelka RC. Effect of antioxidants on x-ray-induced gamma-H2AX foci in human blood lymphocytes: preliminary observations. *Radiology.* 2012;264:59–67.
15. Rübe CE, Grudzenski S, Kuhne M, et al. DNA double-strand break repair of blood lymphocytes and normal tissues analysed in a preclinical mouse model: implications for radiosensitivity testing. *Clin Cancer Res.* 2008;14:6546–6555.
16. Rübe CE, Dong X, Kuhne M, et al. DNA double-strand break rejoining in complex normal tissues. *Int J Radiat Oncol Biol Phys.* 2008;72:1180–1187.
17. Noda A. Radiation-induced unrepairable DSBs: their role in the late effects of radiation and possible applications to biodosimetry. *J Radiat Res (Tokyo).* 2018; 59:ii114–ii120.
18. Horn S, Barnard S, Rothkamm K. Gamma-H2AX-based dose estimation for whole and partial body radiation exposure. *PLoS One.* 2011;6:e25113.
19. Eberlein U, Nowak C, Bluemel C, et al. DNA damage in blood lymphocytes in patients after ^{177}Lu peptide receptor radionuclide therapy. *Eur J Nucl Med Mol Imaging.* 2015;42:1739–1749.
20. Schumann S, Scherthan H, Lapa C, et al. DNA damage in blood leucocytes of prostate cancer patients during therapy with ^{177}Lu-PSMA. *Eur J Nucl Med Mol Imaging.* 2019;46:1723–1732.
21. Denoyer D, Lobachevsky P, Jackson P, Thompson M, Martin OA, Hicks RJ. Analysis of ^{177}Lu-DOTA-octreotate therapy–induced DNA damage in peripheral blood lymphocytes of patients with neuroendocrine tumors. *J Nucl Med.* 2015;56:505–511.
22. Delker A, Fendler WP, Kratochwil C, et al. Dosimetry for ^{177}Lu-DKFZ-PSMA-617: a new radiopharmaceutical for the treatment of metastatic prostate cancer. *Eur J Nucl Med Mol Imaging.* 2016;43:42–51.
23. Sandström M, Garske-Roman U, Granberg D, et al. Individualized dosimetry of kidney and bone marrow in patients undergoing ^{177}Lu-DOTA-octreotate treatment. *J Nucl Med.* 2013;54:33–41.
24. Del Prete M, Buteau FA, Arsenault F, et al. Personalized ^{177}Lu-octreotate peptide receptor radionuclide therapy of neuroendocrine tumours: initial results from the P-PRRT trial. *Eur J Nucl Med Mol Imaging.* 2019;46:728–742.
25. Violet J, Jackson P, Ferdinandus J, et al. Dosimetry of ^{177}Lu-PSMA-617 in metastatic castration-resistant prostate cancer: correlations between pretherapeutic imaging and whole-body tumor dosimetry with treatment outcomes. *J Nucl Med.* 2019;60:517–523.
26. O'Neill E, Kersemans V, Allen PD, et al. Imaging DNA damage repair in vivo after ^{177}Lu-DOTATATE therapy. *J Nucl Med.* 2020;61:743–750.
27. Mariotti LG, Pirovano G, Savage KI, et al. Use of the γ-H2AX assay to investigate DNA repair dynamics following multiple radiation exposures. *PLoS One.* 2013;8:e79541.
28. Fliedner TM, Nothdurft W, Steinbach KH. Blood cell changes after radiation exposure as an indicator for hemopoietic stem cell function. *Bone Marrow Transplant.* 1988;3:77–84.
29. Dainiak N. Hematologic consequences of exposure to ionizing radiation. *Exp Hematol.* 2002;30:513–528.
30. Rothkamm K, Barnard S, Moquet J, Ellender M, Rana Z, Burdak-Rothkamm S. DNA damage foci: meaning and significance. *Environ Mol Mutagen.* 2015;56:491–504.